

# East African Journal of Information Technology

[eajit.eanso.org](http://eajit.eanso.org)

Volume 7, Issue 1, 2024

Print ISSN: 2707-5346 | Online ISSN: 2707-5354

Title DOI: <https://doi.org/10.37284/2707-5354>



EAST AFRICAN  
NATURE &  
SCIENCE  
ORGANIZATION

Original Article

## A Prostate Boundary Localization and Edge Denoising Algorithm

Daisy Thembelihle Mukondiwa<sup>1\*</sup>, Prof. YongTao Shi, PhD<sup>1</sup> & Chao Gao<sup>1</sup>

<sup>1</sup> China Three Gorges University, Yichang, Hubei.

\* Correspondence ORCID ID: <https://orcid.org/0009-0003-3036-9837>; email: [dtee1996mukondiwa@gmail.com](mailto:dtee1996mukondiwa@gmail.com).

Article DOI: <https://doi.org/10.37284/eajit.7.1.1900>

Date Published: **ABSTRACT**

30 April 2024

**Keywords:**

Prostate  
Segmentation,  
TRUS Segmentation,  
Target Localization,  
Boundary Denoising

This research aimed at presenting a two-step method for prostate segmentation in TRUS images. The research used a prostate boundary localization and prostate edge denoising approach. The proposed method contribution is the use of the optimized Hodge's method as the boundary operator and the use of the Bidirectional Exponential moving average to perform edge denoising. The results showed that the proposed method is effective in completing the prostate segmentation task. (1) The prostate region is effectively initialized and localized. (2) The recovery of noise points is accomplished and the segmentation result being consistent with the general shape of the prostate. The experimental results showed that this method can improve the overall segmentation accuracy. The process uses a combination of traditional and unsupervised methods, eliminating the need to rely on large data sets compared to current deep learning methods. The proposed method achieved excellent segmentation accuracy, with the Dice similarity coefficient (DICE) value of 0.9679, an average Intersection over Union (IoU) value of 0.9377, and an average False Positive Rate (FPR) of 0.0399. The results obtained from this study have significant implications for clinical practice. Accurate prostate segmentation is crucial for various applications, including radiation therapy planning, image-guided interventions, and computer-aided diagnosis. The proposed method has the potential to improve these applications by providing more precise and reliable prostate segmentations. However, it is important to acknowledge some limitations of this study. First, the proposed method was evaluated on a limited dataset, which may not fully represent the diversity of prostate images encountered in clinical practice. Further validation on larger datasets is necessary to assess its generalizability. Additionally, the proposed method relied on manual annotations for training, which can introduce inter-observer variability. Incorporating automated or semi-automated annotation techniques could enhance the robustness of the method.

### APA CITATION

Mukondiwa, D. T., Shi, Y. & Gao, C. (2024). A Prostate Boundary Localization and Edge Denoising Algorithm. *East African Journal of Information Technology*, 7(1), 108-120. <https://doi.org/10.37284/eajit.7.1.1900>

### CHICAGO CITATION

Mukondiwa, Daisy Thembelihle, YongTao Shi and Chao Gao. 2024. "A Prostate Boundary Localization and Edge Denoising Algorithm". *East African Journal of Information Technology* 7 (1), 108-120. <https://doi.org/10.37284/eajit.7.1.1900>.

**HARVARD CITATION**

Mukondiwa, D. T., Shi, Y. & Gao, C. (2024) "A Prostate Boundary Localization and Edge Denoising Algorithm", *East African Journal of Information Technology*, 7(1), pp. 108-120. doi: 10.37284/eajit.7.1.1900.

**IEEE CITATION**

D. T. Mukondiwa, Y. Shi & C. Gao "A Prostate Boundary Localization and Edge Denoising Algorithm", *EAJIT*, vol. 7, no. 1, pp. 108-120, Apr. 2024.

**MLA CITATION**

Mukondiwa, Daisy Thembelihle, YongTao Shi & Chao Gao "A Prostate Boundary Localization and Edge Denoising Algorithm". *East African Journal of Education Studies*, Vol. 7, no. 1, Apr. 2024, pp. 108-120, doi:10.37284/eajit.7.1.1900.

**INTRODUCTION**

Prostate cancer is the second most commonly diagnosed cancer and the fifth leading cause of cancer death among men worldwide [1]. The analysis of medical images has become a significant point of focus in computer vision as it has aided in patient diagnosis and treatment strategy especially for cancer treatment and biopsy [1]. In medical research and practice, it is important to accurately measure the shape, borders, and volume of the prostate to obtain information about the pathology of the tissue to aid proper analysis by a medical practitioner. Trans-rectal Ultrasonography (TRUS) has many advantages, including its portability, ease of use, lack of ionizing radiation, low cost, and capability to perform real-time imaging [2].

However, these ultrasound images have several liabilities, including low signal-to-noise ratio, signal loss, scatter, noise, and artefacts during shooting. The result of these liabilities presents themselves in the image as blurred borders and poor visibility of the prostate, and in some cases, no visible borders. In addition, the prostate gland varies in appearance, shape, and size from patient to patient, and even the tissues of the same prostate gland are severely heterogeneous. As a requirement for quantitative analysis in clinical practice, examining the boundaries of the prostate gland is often necessary. The accuracy of the prostate boundary segmentation can impact the formulation of subsequent treatment plans [3]. Computer segmentation was introduced to solve the problems presented by manual segmentation.

**Current State of Research**

Computer-aided image segmentation has been a growing as technology in both the medical field and computer programming field. Under

computer-aided segmentation research in this area has explored automatic and semi-automatic segmentation techniques. The segmentation approaches utilize different concepts to obtain the desired segmentation result. Segmentation methods can be classified according to the theoretical computational approach taken to solve the problem. We can classify the methods as follows: contour and shape based, region based, supervised and unsupervised classification methods based, and hybrid methods. Among these methods are some classified as traditional segmentation methods [4]. These methods are a result of the application of digital image processing concepts and mathematics which are in turn used to segment the image. The calculation is simple, and the segmentation speed is fast, but the accuracy of the segmentation is not ideal in obtaining a highly detailed segmentation result. The ideas of traditional segmentation methods are still worth learning as they can be improved by applying the concepts to modern segmentation methods. The segmentation methods that combine traditional concepts and new techniques are called hybrid methods, many of which beat independent traditional concepts in performance. Currently, deep convolutional neural networks (CNNs) are a common method of use in automated segmentation for both medical and semantic applications.

**RESULTS ON PREVIOUS RESEARCH**

Many researchers [7, 13, 17] have proposed various computer-aided boundary segmentation algorithms. Among the proposed algorithms, deformable models and statistical shape model-based algorithms demonstrated promising segmentation results. Yan et al proposed method automatically extracts prostate boundary from two-dimensional TRUS images for shape

correction in shadow areas [18]. The segmentation process estimates missing boundaries using the partial active shape model.

Deleey et al. [19] also presented a semi-automatic segmentation algorithm that first uses image warping to make the prostate shape elliptical. The method took advantage of the similarity between the prostate shape and the warped ellipse. Although the method is simple and efficient, its application is limited to images in the mid-gland region with regular shapes. In addition, it needs six points selected from specific locations to initialize the algorithm. Ghose et al. [20] and Gong et al. [21] integrated prior knowledge of the potential prostate shapes into their algorithm.

The automatic segmentation procedure of Ghose et al. [20] combined a statistical shape model of the prostate to initialize the prostate shape. This shape was then deformed in an adaptive, hierarchical manner until the technique converged to the final model. Unfortunately, this technique is very expensive computationally, requiring over a minute to segment a single image. Gong et al. [21] modelled the prostate shape by fitting super-ellipses to 594 manually segmented prostate contours. Peng et al. proposed a hybrid segmentation method (H-SegMed) [22] for accuracy. The results of these proposed methods are promising. Still, the drawback of expert intervention is a shared concern as these methods mentioned above require manual expert-provided seed points for initialization.

Deep learning methods have recently been successful in medical imaging for segmenting the anatomy of interest. Segmentation algorithms based on deep learning have been applied to this problem [9]–[15]. Ronneberger et al. [23] proposed a fully convolutional neural network (UNET) with this architecture to work with very few training images and yield more precise segmentation results. Orlando et al. [24] proposed deep learning on clinically diverse 3D ultrasound image segmentation. In the proposed method, 3D segmentation predicted 2D slices, and the modification of 2D U-Net was utilized for training and testing. The method shows that the result of

DSC is 94.1%, and HD is 2.89 mm. Ghavami [15] compared the performance of six different CNN-based algorithms UNet, VNet, HighRes3dNet, HolisticNet, DenseVNet, and Adapted UNet. Deep learning methods are typically efficient, but that is not the consensus. Chen et al [25] highlight the shortcomings of using CNNs to segment biomedical images.

The commonly used loss functions in CNNs generally evaluate pixel-wise similarity. For instance, CE and Dice focus on extracted features from specific regions. While this can result in good classification and segmentation performance, low resultant loss function values may not necessarily correspond to a meaningful segmentation. For example, noisy biomedical images can add many contours in the background representing incorrect segmentation, and object boundaries can be fuzzy due to the difficulty of classifying pixels near the boundary. Chen et al. [7] then proposed an Active contour loss function drawn from Active shape models to be used with CNNs for better results. The loss function (or cost function) plays a significant role in training a CNN model. Loss function measures the error of prediction or segmentation which can be back propagated to previous layers to update the weights. The advantage of this new loss function is that it can seamlessly combine the geometrical information (e.g. boundary length) with region similarity thus leading to more precise segmentation. Several approaches similar have been proposed that combine deformable models with neural networks (NNs) to improve boundary detection. A deep Convolutional Neural Network (CNN) was used by Zhang et al. [26] to integrate a well-trained model to detect and classify tumour nodules. Competitive results were also achieved by Kasinathan et al. [27] through the combination of CNN and active contours to detect and classify 3D lesion lung tumour CT images automatically. In the above examples we see the application of segmentation methods based on deep learning being used in conjunction with prior shape knowledge to make them effective for the complex task of biomedical image segmentation.

Deep learning methods are limited in performance in medical image segmentation task. For them to be effective large amounts of data that accurately represent the variability in the data are needed. Prior shape knowledge helps compensate for the noise in the image and reduces the amount of training data needed to accurately train the model for accurate segmentation results. Nevertheless, the general ramifications of using deep learning models are still relevant. A significant amount of time is needed to train the network, the computational complexity and cost of these deep learning models still apply. In this paper we apply mathematical principles to solve this segmentation problem. Therefore, our model can be a better substitute in this task as it will take less time to train and less resources to implement, without compromising performance excellence.

## MATERIALS AND METHODS

The proposed method is a hybrid approach containing application of machine learning based models (RF, DAE) and mathematical models (Improved normal vector, BDEMA). The study utilised accurate segmentation for precise measurements, localization of abnormalities, and treatment planning using machine learning technique for prostate segmentation in TRUS images. This method consists of two crucial steps, prostate boundary localization and prostate boundary denoising. The localization is done by the Random forest algorithm and Denoising Auto-encoder (DAE). Furthermore, the boundary operator used for this step is an improved normal vector boundary operator. The second step used the Bidirectional Exponential moving average (BDEMA) to denoise the boundary. The proposed method for prostate segmentation in TRUS images shown in the flow chart is a two-step method. In the first step, an improved Normal vector boundary operator (Improve Hodges method) is used to localize prostate boundary points using the information from the RF and DAE (Section b of the method). The second step uses the BDEMA method in denoising the prostate boundary, a crucial aspect of determining noise points by the use of a threshold value also added to this step (Section c of the method).

## METHOD

### Section A: Localization

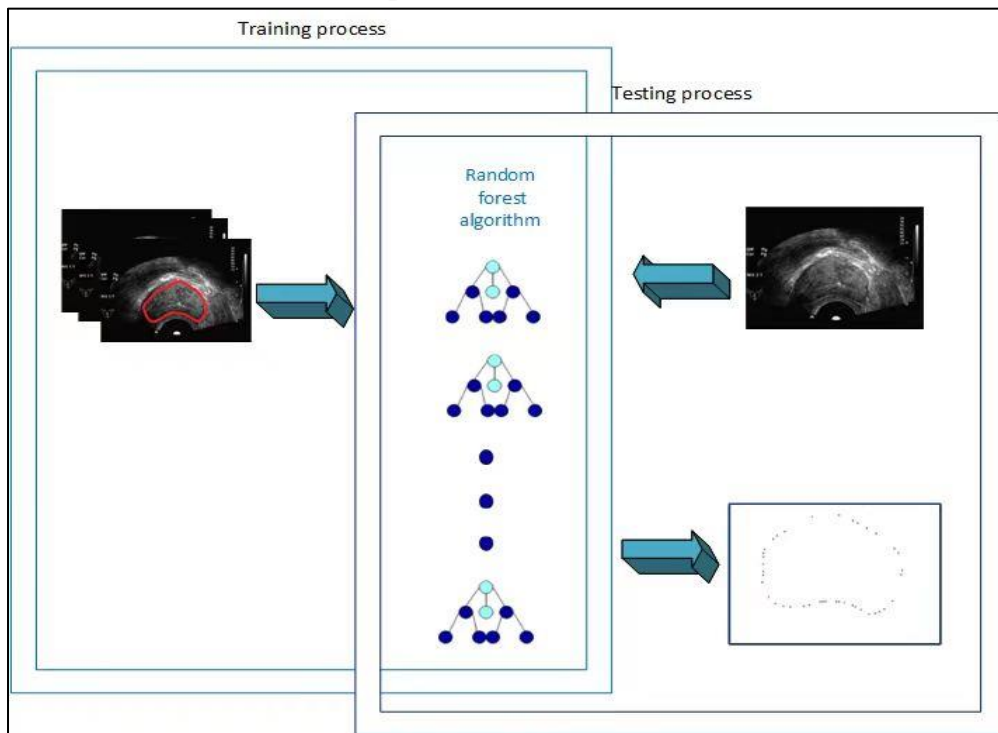
Foundation of localization: In the field of image segmentation, the edge shape of an object is usually represented as a closed curve or as a collection of points sampled on a closed curve, and the contour of an object is described by the line segments connected between the points. This is done by the random forest, and this is shown in *Figure 1*. When the set of points are too sparse to accurately describe/show/embodiment the contour of an object, it is necessary to supplement the point positions in such a way that the distribution of the points is known/clear, for example, by their shape, and then to form a new set of points by combining the supplemented point positions to recover the high-precision description of the object. This is done by the denoising auto-encoder and shown in *Figure 2*.

### Random Forest Process

The model is based on a random forest model of the location of the prostate gland, where  $J_i$  is the set of all image coordinates for the  $i^{\text{th}}$  pixel,  $J_i \{img, character, label\}$ , where  $img$  is the set of all pixel points,  $img_i$  is the set of all image coordinates for the  $i^{\text{th}}$  pixel, and  $character$  is the image feature defined as  $character = \{m, d, orient\}$ . The label is a description of whether or not the current pixel is a true border point.  $orient = \{orient_1, orient_2, \dots, orient_8\}$  it is the sum of the grayscales counted for the current pixel point extending  $len$  lengths into the 8 neighborhoods,  $m$  is the mean of  $orient$ ,  $d$  is the variance of  $orient$  and  $len$  is usually set depending on the size of the pixel noise region.

The training dataset is randomly sampled, and a subset of features is randomly selected from  $J_i$  to generate a sub-decision tree with information gain, so as to obtain a random forest that can generate boundary points from the image information.

**Figure 1: Random Forest process image. This image summarizes the input, training and expected outcome of this localization step.**



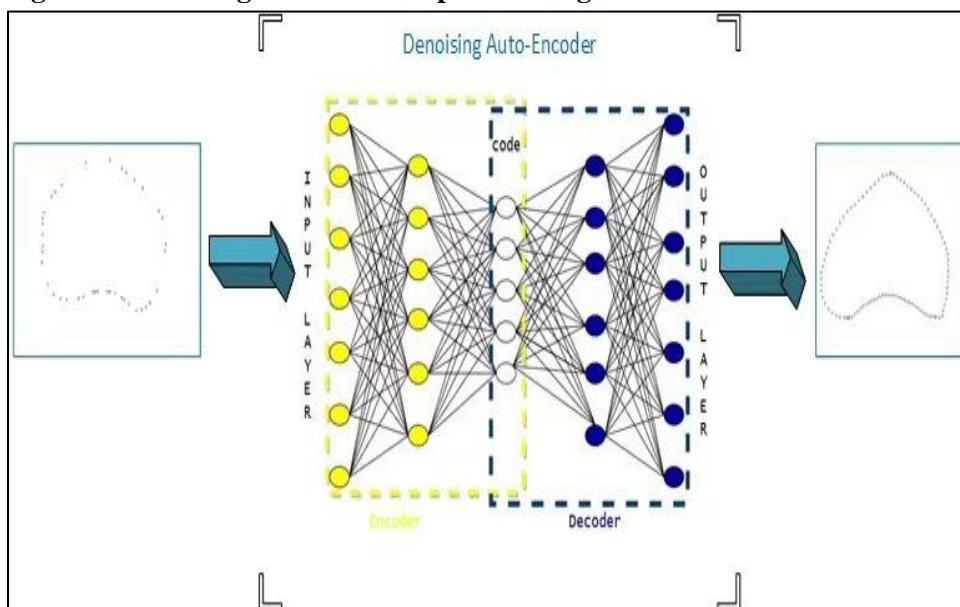
Source: Breiman (2001, p 78)

**Denoising Autoencoder Process**

During the training phase, the denoising autoencoder is presented with pairs of noisy input and their corresponding clean versions. The encoder network maps the noisy input image to a lower-dimensional representation, while the

decoder network reconstructs the clean output from this representation. The ability of a denoising autoencoder to recover contours using learned distribution stems from its ability to capture the underlying structure and patterns in the data.

**Figure 2: Denoising Auto-encoder process diagram**



Source: Breiman (2001, pp 101)

**Denosing Auto-encoder (DAE).** If there exist two mapping relations  $f(x)$ ,  $g(x)$ , where  $f(x)$  is the encoder and  $g(x)$  is the decoder function. Equation 1 constructs a two-dimensional vector to describe the prostate boundary as a planar shape  $x$ . The following equations can describe the process:

Encoder:

$$z = f(Wx + b) \quad (2)$$

Where  $x$  is the input,  $W$  is the weight matrix,  $b$  is the bias vector,  $f$  is the activation function, and  $z$  is the compressed representation.

$$z' = z + n \quad (3)$$

Where  $n$  is the noise added to the input.

Decoder:

$$x' = g(W'z' + b') \quad (4)$$

Where  $W'$  is the transpose of  $W$ ,  $b'$  is the bias vector for the decoder,  $g$  is the activation function for the decoder, and  $x'$  is the denoised output.

$$L(x, x') = \|x - x'\|^2 \quad (5)$$

Where  $L$  is the loss function that typically measures the difference between the input and output.

Describing a curve as a set of points is an approximation, and the interpolated distance between points should not be considered a loss function. It is, therefore, more realistic to use either the tessellation distance (D8 distance) or the point-to-line distance to describe the situation. Let  $p$  be the reconstruction boundary point, and  $q(s, t)$  be the loss function at point  $p$  for the subject pixel that is first found by the pixel information extractor in the pixel 8 neighbourhood loop. The distance between the two points is taken as the loss function, then the loss should be as shown in equation 6, which gives the total loss for a single sample as shown in equation 7.

$$L(p) = D(p, q) = \sqrt{(x_p - s)^2 + (y_p - t)^2} \quad (6)$$

$$\rightarrow L(z) = \sum_{i=1}^n \sqrt{(z_i - s)^2 + (z_i - t)^2} \quad (7)$$

The goal of training a denosing auto-encoder is to minimize this loss function by adjusting the weights and biases of both the encoder and decoder. In our case, the task of this auto-encoder is to construct a full set of boundary points based on the 'seed points' from the previous step by filling in the missing points with zeros and feeding them together with the points from the previous step into the trained encoder. This results in a fully reconstructed boundary point set  $x$ .

## Section B: Improved Normal Vector Contrast to Optimize Localization.

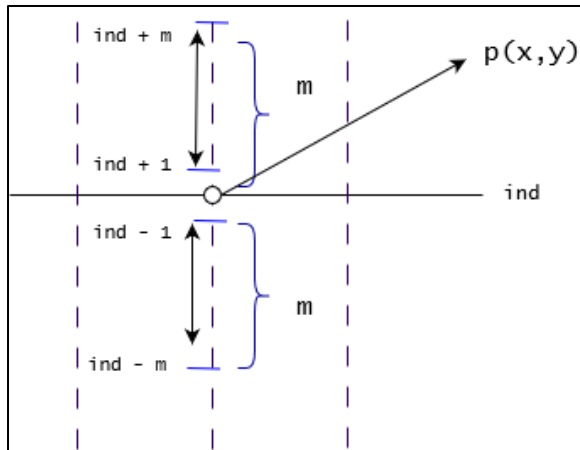
**Normal Vector Contrast.** Since the contrast of the target boundary in an ultrasound image is low, traditional boundary operators such as Sobel and Robert cannot detect this type of boundary. As a result, Hodge [21] proposed a boundary operator called the normal vector contrast boundary operator, which improves the conventional boundary operator to detect target boundaries in ultrasound images. Representing the split curve as a set of points  $x$  as given previously. Let us assume that the normal vector at a point  $(x, y)$  on the curve is represented by  $n$  and its direction is specified to point to the outside of the curve. Define the vector along the positive and negative directions of the normal vector at the point, of which is the gray level of the image of the point on the normal vector, the coordinates of which are.

This is equivalent to finding the cumulative gray level difference of the point along the normal vector in a certain range, with the target boundary point located at the location with the largest gray level difference. By traversing all points on the curve in this way, the approximate boundary of the target can be obtained.

The Hodges normal vector boundary operator is specifically designed to extract boundaries or

contours from medical images. It operates by computing the normal vectors at each point on the boundary of an object in the image. These normal vectors represent the direction perpendicular to the boundary surface at each point. This is shown in *Figure 3* below.

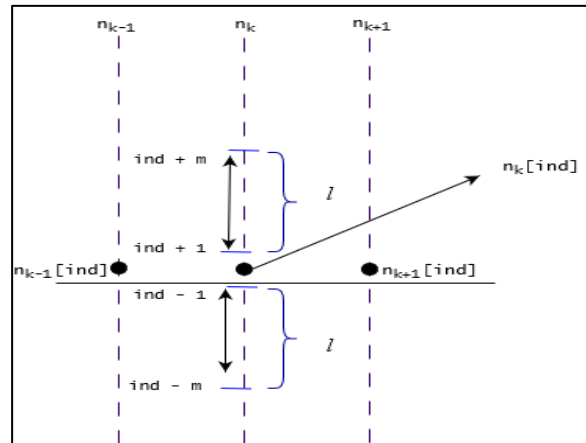
**Figure 3: Normal vector contrast diagram**



An improved version of Hodge’s method is used in this paper instead of the original method. The boundary operator  $C$  is further improved to take into account the neighbouring points information of other segments before and after a segmentation point  $n_k[ind]$ , and to correct the position of  $n_k[ind]$ .

As shown in *Figure 3*, the three normal vectors of  $n_k$  and its neighbours  $n_{k-1}$  and  $n_{k+1}$  are made and locally enlarged for ease of description. The point on the normal vector  $n_k$  with row index  $ind$  can be represented as  $n_k[ind]$ , and the points on the normal vectors of its preceding and following neighbours with the same index are identified in *Figure 3-13* and can be represented as  $n_{k-1}[ind]$  and  $n_{k+1}[ind]$  respectively. The boundary operator for the point  $n_k[ind]$  is shown in *Figure 4* below which is:

**Figure 4: Improved normal vector diagram.**



$$C_{neigh} = \sum_{m=k-l}^{k+l} C_{ind} \quad (3-1)$$

In Equation (3-1),  $l$  represents the number of unilateral neighboring points at point  $n_k[ind]$  and  $m$  represents the number of normal vectors in the neighborhood section.

This equation calculates the difference in grayscale between the upper and lower bounding boxes shown in *Figure 3-13*, rather than just the grayscale information on the single normal vector. Therefore, the boundary operator  $C_{neigh}$  contains much more gray information than  $C$ , thus avoiding the creation of noisy segmentation points due to local gray noise at a few segmentation points.

### Section C: Denoising

Due to the current limitations of using only the gray level to assert the position of the boundary, we need to consider the semantic information before and after the boundary, which is well implied by other points. However, the direct use of the EMA technique is not ideal because it only provides the trend of the current position compared to the position of preceding points and does not consider the successive points. In short, when we consider any point in the one-way sequence, the one-way sequence is consistently unable to consider the latter information. The equation for calculating the BEMA is given by:

$$EMA_t = \alpha x_t + (1 - \alpha) EMA_{t-1} \quad (9)$$

Where is the data point at time  $t$ ,  $\alpha$  is the smoothing factor that determines the weight given to the current data point, and is the EMA value at the previous time step.

This method's result is highly sensitive to outliers. That is, the information from the outliers can affect the weights used on the successive points leading to distortion of the general shape. So, we propose a way that any point can refer to the grayscale proposals on both sides of the preceding and successive point simultaneously.

We, therefore, propose a Bidirectional EMA (BEMA).

The algorithm is formulated as follows:

$$BDEMA_t = \alpha x_t + \beta x_{t+1} + \gamma x_{t-1} + (1 - \alpha - \beta - \gamma)BDEMA_{t-1}. \quad (10)$$

Where  $x_{t+1}$  and  $x_{t-1}$  are the successive and preceding data points, respectively, and  $\alpha$ ,  $\beta$ , and  $\gamma$  are the smoothing factors that determine the weights given to each data point.

#### Section D: Innovation of the Method

The innovation of this study is the use of improved Hodge's method as a boundary operator and the use of the BDEMA to denoise the identified noise points.

**Table 1: Evaluation metrics table for six images used in the experiment**

Image index	MAE	DSC	IoU	FPR	Run Time
a	1.1145	0.9706	0.9426	0.0311	0.3567s
b	1.4554	0.9647	0.9319	0.0392	0.1423s
c	0.4163	0.9686	0.9386	0.0118	0.3123s
d	0.7683	0.9663	0.9343	0.0238	0.2124s
e	0.6127	0.9786	0.9585	0.0163	0.2246s
f	2.0951	0.9686	0.9203	0.0813	0.3205s

The results shown above in *Table 1* show the performance of the proposed method according to the selected evaluation metrics. These results are the results of six images in the data set, the images are labelled from index a-f. We can therefore calculate an average value of each of the metrics of the proposed method, from table 5-1 the average IoU is 0.9377, the average DSC is 0.9679, the average MAE is 1.07205, the average FPR is 0.0399 and average runtime is 0.28975s.

#### Section E of the Method: MATERIALS

The data set used in this study consists of ultrasound images of the prostate that were taken from real clinical examination data of a hospital, and the true boundaries of the prostate gland were annotated by a professional doctor as the Ground Truth of the target boundary for subsequent evaluation of the segmentation performance. A total of blank TRUS images were used, and 132 images with a resolution of  $576 \times 768$  pixels were used for the test, each with a pixel size of  $0.138 \text{ mm} \times 0.138 \text{ mm}$ . The experimental platform relies on PaddlePaddle. The relevant platform parameters are platform: Linux, Python: 3.7.4, GPU: Tesla V100-SXM2-32GB. To quantitatively evaluate the experimental results obtained by our method, we decided to compare the mean absolute error (MAE), Dice Similarity Coefficient (DSC), Intersection over Union (IoU), False Positive Rate (FPR), and Runtime.

#### RESULTS AND DISCUSSION

Table 1 shows the performance result of our method based on the five-performance metrics chosen. False Positive Rate (FPR), Dice Similarity Coefficient (DSC), Mean Absolute Error (MAE), Intersection over Union (IOU) and Run Time.

We can therefore go further and tally the results of our proposed method to that of other state of the art methods in *Table 2*. When evaluating the performance of prostate segmentation methods, it is important to compare the results with other state-of-the-art techniques. In this case showing the effectiveness of our proposed method to yield good results in comparison to other methods. The methods chosen for this comparison all fall under the deep learning methods of segmentation

mentioned in the introduction of this paper. The shortcomings of deep learning methods in the segmentation problem of this paper where a motivation for a non-deep learning-based method to be proposed. Therefore, the evaluation of the

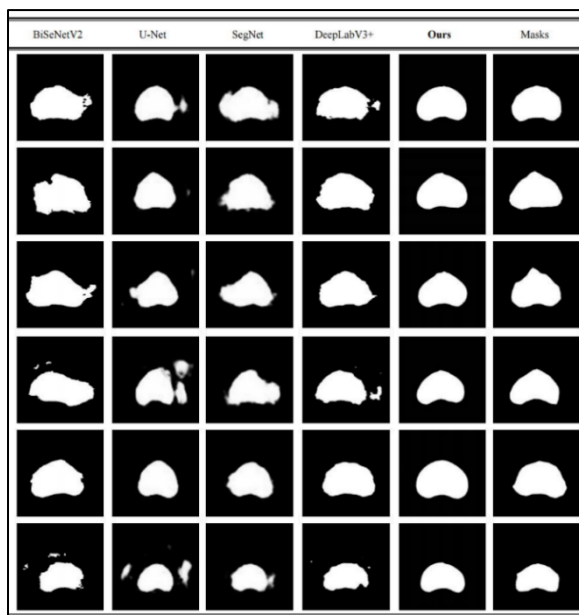
proposed method has to be tallied against the well performing deep learning-based methods in order to highlight the effectiveness of the proposed method that evades the complexities of the deep learning methods.

**Table 2: Table of comparison of our method and other state of the art methods based on three performance metrics Dice Similarity Coefficient (DSC), Intersection Over Union (IOU) and False Positive Rate.**

Method	DSC	IoU	FPR
BiSeNetV2[43]	0.8387	0.7223	0.1119
U-Net [21]	0.8877	0.8069	0.0831
SegNet [19]	0.8584	0.7597	0.0888
DeepLabV3+[42]	0.9522	0.9117	0.0592
Our Proposed Method	0.9679	0.9377	0.0399

The segmentation results in Figure 5 show that the neural network segmentation method is prone to the phenomenon of outliers or blurred boundaries. For example, the U-net segmentation results of images d and f in Figure 5 are shown. For SegNet and BiSeNetV2 the overall shape of the result is affected by these. Although the segmentation result of DeepLabV3+ is better and the IoU is as high as 91%, it still cannot avoid the above shortcomings, as shown in Figure 5 for image a and image d.

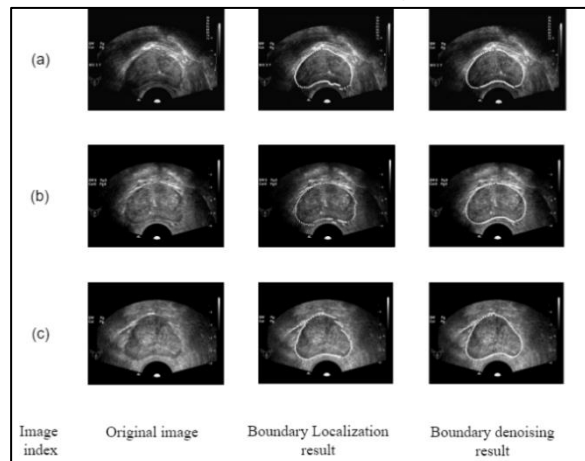
**Figure 5: Segmentation results of BiSeNetV2, U-Net, SegNet, DeeplabV3+, Our method and masks.**



The following is a sample picture showing table of results of the two-step proposed method. It

shows the original image, localization result and denoising result.

**Figure 6: Table of results of the two-step proposed method. It shows the original image, localization result and denoising result.**



## CONCLUSION

The methods proposed in this paper can be described as a two-step prostate boundary segmentation algorithm. This paper uses random forest, denoising auto-encoder and an improved normal vector boundary operator in prostate boundary localization. In the boundary localization step most of the boundary points are accurately detected, and most of them are already at the real boundary points, except for a few points (called noise points, which correspond to artifacts or low signal-to-noise regions). In the boundary denoising section of the paper there is outlier detection and outlier realignment by the use of the

bidirectional exponential moving average (BDEMA). The results show that the proposed method is effective in completing the prostate segmentation task. (1) The prostate region is effectively initialized and localized. (2) The recovery of noise points is accomplished and the segmentation result being consistent with the general shape of the prostate. The experimental results show that this method can improve the overall segmentation accuracy. The process uses a combination of traditional and unsupervised methods, eliminating the need to rely on large data sets compared to current deep learning methods.

#### AUTHOR'S CONTRIBUTIONS

**Daisy Thembelihle Mukondiwa:** Research, Experiments, data analysis, written report, written manuscript.

**Professor Shi YongTao:** Supervision, data analysis, proof- read.

**Gao Chao:** Experiment resources, proof-read.

#### REFERENCES

- [1] M. A., Kasban, Hany, M. El-Bendary, and D. H. Salama. "A comparative study of medical imaging techniques", *International Journal of Information Science and Intelligent System*, Vol. 4, issue 2, pp 37-58, 2015.
- [2] Y., Wang, J. Z., Cheng, Z., D., Ni. et al. "Towards Personalized Statistical Deformable Model and Hybrid Point Matching for Robust MR-TRUS Registration. [M]". *Springer International Publishing*, Vol. 20, issue 6, pp 807-58, 2016.
- [3] K.K., Hodge, J.E., McNeal, M.K., Terris, T.A., Stamey. "Random systematic versus directed ultrasound guided transrectal core biopsies of the prostate". *Journal Urol.* Vol. 142, issue 1, pp 71-4; discussion 74-5, July 1989.
- [4] Y., Gao, et al. (2018). "A Modified Level Set Method for Prostate Segmentation in MRI." *Journal of Medical Imaging and Health Informatics*, vol. 8, no. 1, pp. 108-115. (Print)
- [5] M., Ghafoorian, N., Karssemeijer, T., Heskes, I.W.M., van Uden, C.I., Sanchez, G., Litjens et al. "Location Sensitive Deep Convolutional Neural Networks for Segmentation of White Matter Hyperintensities". *Sci Rep*, vol. 7, issue 1, 2017.
- [6] B.V., Ginneken, C.M., Schaefer-Prokop, M., Prokop. "Computer-aided Diagnosis: How to Move from the Laboratory to the Clinic". *Radiology*. Vol. 261, issue 3, pp 719–32, 2011.
- [7] X., Chen, B.M., Williams, R., S., Vallabhaneni, G., Czanner, R., Williams, and Y., Zheng. "Learning active contour models for medical image segmentation." In *Proceedings of the conference on Computer vision and pattern recognition, IEEE/CVF*, 2019, pp. 11632-11640.
- [8] F., Liao, M., Liang, Z., Li et al. "Evaluate the malignancy of pulmonary nodules using the 3D Deep Leaky Noisy-or Network". 2017. *arXiv preprint arXiv:1711.08324*.
- [9] L., Chen, Z., Yukun, G., Papandreou, F. Schroff, and A., Hartwig. "Encoder-decoder with atrous separable convolution for semantic image segmentation." In *Proceedings of the European conference on computer vision (ECCV)*, 2018, pp. 801-818.
- [10] A. A. A., Setio, A., Traverso, de Bel T et al. "Validation, comparison, and combination of algorithms for automatic detection of pulmonary nodules in computed tomography images: The LUNA16 challenge". *Med Image Anal*, Vol. 42, pp 1–13, 2017.
- [11] T.F., Cootes, C.J., Taylor, D.H., Cooper, and J. Graham. "Active shape models-their training and application. Computer vision and image understanding", *Med Image Anal*, Vol. 61, issues 1, pp 38-59, 1995.
- [12] B., Etienne (2021), Introduction to machine learning, Wolfram Media, Incorporated, Chapter 7, [Online], Available: <https://books.google.co.uk/books?id=x6K7zgEACAAJ>

- [12] X., Gao, S., Ya, L., Xuelong, and T., Dacheng. "A review of active appearance models, *IEEE Transactions on Systems, Man, and Cybernetics, Part C (Applications and Reviews)*, Vol. 40, issue 2, pp 145-158, 2010.
- [13] M., Zhen, J., Manuel, R.S., Tavares, R. N., Jorge, and T. Mascarenhas. "A review of algorithms for medical image segmentation and their applications to the female pelvic cavity". *Computer Methods in Biomechanics and Biomedical Engineering*, Vol. 13, issue 2, pp 235-246, 2010.
- [14] N., Ghavami, H., Yipeng, E. Gibson, E. Bonmati, M., Emberton, C.M., Moore, and D.C., Barratt. "Automatic segmentation of prostate MRI using convolutional neural networks: Investigating the impact of network architecture on the accuracy of volume measurement and MRI-ultrasound registration". *Medical image analysis*, Vol. 58, pp 1015-58, 2019.
- [15] P., Wu, Y., Liu, Y., Li et al. Robust prostate segmentation using intrinsic properties of TRUS images[J]. *IEEE transactions on medical imaging*, Vol. 34, issue 6, 2015.
- [16] X., Yuan, T., Xu, H., Zhang, L. R., Long, and X., Huang. "Segan: Adversarial network with multi-scale l1 loss for medical image segmentation", *Neuro-informatics*, Vol. 16, 383-392, 2018.
- [17] Yan P, Xu S, Turkbey B, et al. "Discrete Deformable Model Guided by Partial Active Shape Model for TRUS Image Segmentation[J]". *IEEE Trans Biomed Eng*, Vol.57 issue, 5), pp 1158-1166, 2010.
- [18] M.A., Deeley, Chen, A., Datteri, R., Noble, J.H., Cmelak, A.J., Donnelly, E.F., et al. "Comparison of manual and automatic segmentation methods for brain structures in the presence of space-occupying lesions: a multi-expert study", *Phys Med Biol.*, Vol. 56, issue 14, pp 4557-7, 2011
- [19] S., Ghose, O., Arnau, R., Martí, X., Lladó, Joan C. et al. "A survey of prostate segmentation methodologies in ultrasound, magnetic resonance and computed tomography images", *Computer methods and programs in biomedicine*, Vol. 108, issue 1, pp 262-287, 2012.
- [20] L., Gong, D., Sayan, D.R., Pathak, P.S., Cho, and K., Yongmin. "Parametric shape modeling using deformable superellipses for prostate segmentation. "IEEE transactions on medical imaging Vol. 23, issue 3, pp 340-349, 2004.
- [21] T.X., Peng, T., Wang, Y., Fanzhang et al. (2020). Deep Belief Network and Closed Polygonal Line for Lung Segmentation in Chest Radiographs. *The Computer Journal*. Vol. 65, issue 10, pp 89-103
- [22] O., Ronneberger, P., Fischer, and T., Brox. "U-net: Convolutional networks for biomedical image segmentation." In 18th International Conference on Medical Image Computing and Computer-Assisted Intervention–MICCAI, Munich, Germany, October 5-9, 2015, Proceedings, Part III 18, pp. 234-241. *Springer International Publishing*, 2015.
- [23] N., Orlando, D.J., Gillies, I., Gyacskov, C., Romagnoli, D., D'Souza, and A., Fenster. "Automatic prostate segmentation using deep learning on clinically diverse 3D transrectal ultrasound images. "Medical physics, Vol. 47, issue 6, pp 2413-2426, 2020.
- [24] J., Chen and R., Xukan. "Deep learning with edge computing: A review. "Proceedings of the IEEE 107, no. 8 (2019): 1655-1674 Gondara, Lovedeep. "Medical image denoising using convolutional denoising autoencoders." In 2016 IEEE 16th international conference on data mining workshops (ICDMW), pp. 241-246. IEEE, 2016.
- [25] C., Zhang, X., Sun, K., Dang, Li, K., Guo, X.W., Chang, J., Yu, Z.Q., Huang, F.Y., Wu,

- Y.S., Liang, Z., Liu, Z.Y., Zhang, X.G., Gao, X.L., Huang, S.H., Qin, J., Feng, W.N., Zhou, T., Zhang, Y.B., Fang, W.J., Zhao, M.F., Yang, X.N., Zhou, Q., Wu, Y.L., Zhong, W.Z., "Toward an Expert Level of Lung Cancer Detection and Classification Using a Deep Convolutional Neural Network". *Oncologist*. 2019 Sep;24(9):1159-1165. doi: 10.1634/theoncologist.2018-0908. Epub 2019 Apr 17. PMID: 30996009; PMCID: PMC6738288
- [26] G., Kasinathan, J., Selvakumar, H., Amir Gandomi, R., Manikandan, S.J., Fong, and R., Patan. "Automated 3-D lung tumour detection and classification by an active contour model and CNN classifier. "Expert Systems with Applications, Vol. 134, pp 112-119, 2019.
- [27] A.C., Hodge, A., Fenster, D.B., Downey, and H.M., Ladak. "Prostate boundary segmentation from ultrasound images using 2D active shape models: Optimisation and extension to 3D."Computer methods and programs in biomedicine Vol. 84, issue 2-3, pp 99-113, 2006.
- [28] T., Hastie, R., Tibshirani, J.H., Friedman, and J.H. Friedman. "The elements of statistical learning: data mining, inference, and prediction". Vol. 2. New York: springer, 2009.
- [29] M., Liang, W., Tang, X., Xu, et al "Comparison of manual and computer-aided liver tumour segmentation methods for MR images". *J Digit Imaging*, Vol. 27(6), pp 729-736, 2014.
- [30] L., Xiangbin, L., Song, S., Liu, and Y., Zhang. "A review of deep-learning-based medical image segmentation methods", *Sustainability*, Vol. 13, issue 3, pp 1224, 2021.
- [31] M., Mirza, X., Bing, D., Warde-Farley, O., Sherjil, A., Courville, Y., Bengio, I. J. Goodfellow, and J. Pouget-Abadie. "Generative adversarial nets. Advances in neural information processing systems, Vol. 27, pp 2672-2680, 2014.
- [32] M.T., Michael. *Machine learning*. Vol. 1. New York: McGraw-hill, 2007.
- [33] O., Nobuyuki. "A threshold selection method from gray-level histograms", *IEEE transactions on systems, man, and cybernetics*, Vol. 9, issue 1, pp 62-66, 1979.
- [34] V., Gulshan, L., Peng, M., Coram et al. "Development and validation of a deep learning algorithm for detection of diabetic retinopathy in retinal fundus photographs". *JAMA*, 316: pp 2402–2410, 2016.
- [35] S., Rahnamayan, H.R., Tizhoosh, and M.M.A., Salama. "Automated snake initialization for the segmentation of the prostate in ultrasound images." *In Image Analysis and Recognition: Second International Conference, ICIAR, Toronto, Canada*, Springer Berlin Heidelberg, September, 2005. Proceedings 2, pp. 930-937.
- [36] D.E., Rumelhart, G.E., Hinton, and R.J., Williams. "Learning representations by back-propagating errors", *Nature*, 323, no. 6088, pp 533-536, 1986.
- [37] S., Saradwata, and D., Sudipta. "A review of imaging methods for prostate cancer detection: supplementary issue: image and video acquisition and processing for clinical applications." *Biomedical engineering and computational biology* 7, BECB-S34255, 2016.
- [38] J.L., Speiser, M.E., Miller, J., Tooze et al. "A comparison of random forest variable selection methods for classification prediction modeling. Expert systems with applications", Vol. 134, pp 93-10, 2019.
- [39] L.A., Torre, F., Bray, R.L., Siegel, J., Ferlay, J., Lortet-Tieulent, and A., Jemal. "Global cancer statistics, 2012." *CA: a cancer journal for clinicians*, Vol. 65, issue 2, pp 87-108, 2015.

- [40] V., Pascal, et al. "Extracting and composing robust features with denoising autoencoders." *Proceedings of the 25th international conference on Machine learning*. ACM, 2008.
- [41] Wang, G., Li, W., Aertsen, M., Deprest, J., & Ourselin, S. (2019). Automatic fetal brain segmentation from 2D MRI slices for motion correction. *Medical Image Analysis*, 52, 291-303. (Web)
- [42] L., Wang, L., Bin, H., Mengjie, Y., Wang, Z., Wang, and L., Du. (2022). "Prostate cancer incidence and mortality: global status and temporal trends in 89 countries from 2000 to 2019." *Frontiers in Public Health*, Vol. 10, issue 1, pp 811-44, 2019.
- [43] Y., Changqian, G., Changxin, J., Wang, G., Yu, C., Shen, and N., Sang. "Bisenet v2: Bilateral network with guided aggregation for real-time semantic segmentation." *International Journal of Computer Vision*, Vol. 129, pp 3051-3068, 2021.
- [44] Yu, L., Yang, X., Chen, H., Qin, J. & Heng, P.-A. Volumetric ConvNets with mixed residual connections for automated prostate segmentation from 3D MR images. In *AAAI Conference on Artificial Intelligence*, 31, 2017.
- [45] Han, C., Zhu, L., Liu, X. et al. Differential diagnosis of uncommon prostate diseases: combining mpMRI and clinical information. *Insights Imaging*, 12, 79 (2021). <https://doi.org/10.1186/s13244-021-01024-3>.